Spectral butterfly, mixed Dirac-Schrödinger fermion behavior, and topological states in armchair uniaxial strained graphene

Pedro Roman-Taboada* and Gerardo G. Naumis

Departamento de Física-Química, Instituto de Física, Universidad Nacional Autónoma de México, Apartado Postal 20-364, 01000 México, Distrito Federal, Mexico

(Received 9 September 2014; revised manuscript received 30 October 2014; published 21 November 2014)

An exact mapping of the tight-binding Hamiltonian for a graphene nanoribbon under any armchair uniaxial strain into an effective one-dimensional system is presented. As an application, for a periodic modulation we have found a gap opening at the Fermi level and a complex fractal spectrum, akin to the Hofstadter butterfly resulting from the Harper model. The latter can be explained by the commensurability or incommensurability nature of the resulting effective potential. When compared with the zig-zag uniaxial periodic strain, the spectrum shows much bigger gaps, although in general the states have a more extended nature. For a special critical value of the strain amplitude and wavelength, a gap is open. At this critical point, the electrons behave as relativistic Dirac fermions in one direction, while, in the other direction, a nonrelativistic Schrödinger behavior is observed. Also, some topological states were observed which have the particularity of not being completely edge states since they present some amplitude in the bulk. However, these are edge states of the effective system due to a reduced dimensionality through decoupling. These states also present the fractal Chern beating observed recently in quasiperiodic systems.

DOI: 10.1103/PhysRevB.90.195435 PACS number(s): 73.22.Pr, 71.23.Ft, 03.65.Vf

I. INTRODUCTION

Graphene is an amazing one-atom-thick material. Its remarkable properties include high mobility, anomalous Hall quantum effect, Klein tunneling, lack of backscattering, etc. [1]. Moreover, graphene possesses excellent mechanical properties, such as, for example, the largest known elastic response interval (up to 25% of the lattice parameter [2]). The importance of this stems from the fact that it is possible to modify the electronic properties of graphene using elastic deformations, leading to a new field called "straintronics" [3–6]. For example, strain can modify electron-phonon coupling and even superconductivity [7]. In the literature, several approaches are used [5,8,9]. The most common one is to combine a tight-binding Hamiltonian with linear elasticity theory [8,10–12]. Under this approach, high pseudomagnetic fields appear, although assuming that the Dirac cone is not significantly modified [13]. However, for certain conditions that occur experimentally, like in graphene grown on top of a crystal [14] or rotated crystals [15], a gap can be opened at the Fermi level [16]. Such gaps are not obtained under the physical limit considered in the pseudomagnetic field approach, although it has a paramount importance for technical applications. Using other approaches, it has been shown that the induced gap opening depends strongly upon the direction of the strain [3] and requires values as large as 23%.

In a previous publication [16], we found a general method to map any zig-zag uniaxial strain into a one-dimensional effective system. Such a map opened the possibility to study strain from a new perspective. For example, we have proved that, in certain circumstances, periodic uniaxial strain produces a quasiperiodic behavior, due to the incommensurability of the effective resulting potential [16]. This results in a kind of modified Harper model [17]. The original Harper model leads to the Hofstadter butterfly [18], which arises in the problem of an electron in a lattice with an applied uniform magnetic field. At the same time, these kinds of rough ideas were experimentally confirmed for graphene on top of hexagonal boron nitride as the rotational angle between the two hexagonal lattices was changed [15].

Unfortunately, in our previous work [16] we found that the gap sizes were very small and required strain amplitudes as large as 20% of the interatomic distance. This was a little bit disappointing from the technological point of view, as well as for studying the topological properties [19]. Since it is known that graphene under uniaxial uniform armchair strain presents a bigger gap opening at the Fermi level than zig-zag graphene [3], we decided to investigate the effects of a different kind of strain. As we will see throughout this paper, we found that it is possible to generate much bigger gaps using graphene nanoribbons under uniaxial armchair periodic elastic strain. Moreover, during this study we found an interesting effect at a critical point where a gap is open. At this point, the electrons have a mixed behavior. In one direction, a relativistic Dirac dynamics is followed, while, in the other direction, a nonrelativistic Schrödinger behavior is seen; i.e., the Dirac cone has a distorted cross section. As we will see, this results from a decreasing of the effective dimensionality due to strain. In fact, such behavior was theoretically anticipated by tuning *ad hoc* the graphene parameters [20,21]. Although Montambaux and coworkers [21] found since 2009 that bond pattern changes can result in a Dirac-Schrödinger behavior, there was not available an experimental setup to produce such a pattern. Here we prove that, in fact, such a possibility can be realized with the most simple oscillating strain. Our paper shows that armchair strain is needed to produce a transition to the Dirac-Schrödinger behavior, which is not observable using the zig-zag case.

This also opens the way to study interesting topological properties of the resulting one-dimensional effective systems [19]. We would like to point out that many of the results

*peter89@fisica.unam.mx

presented in this paper are different from our previous work on zig-zag. In particular, the special kind of topological states found here are almost impossible to be observed in the zig-zag strain case because the gaps do not open or are very small for realistic values of strain.

Finally, it is important to discuss the possibility of having an experimental system with the proposed uniaxial stain. From this point of view, is clear that in order to have such strain one needs to solve the elastic equations to derive the appropriate stress load. By using this kind of experimental setup, it can be difficult to get the proposed uniaxial strain, as we will discuss later on. A much better prospect is to grow graphene on top of another lattice, in which it has been demonstrated in some particular cases that the strain is uniaxial [14,22]. Other systems that are suitable to observe the proposed effects are artificially made graphene superlattices [23–25], in which strain can be designed at will.

II. MAPPING OF ARMCHAIR UNIAXIAL STRAIN INTO AN EFFECTIVE ONE-DIMENSIONAL SYSTEM

When graphene is loaded with external forces, a strain pattern results. The new positions of the carbon atoms in the strained graphene are given by

$$\boldsymbol{r}' = \boldsymbol{r} + \boldsymbol{u}(\boldsymbol{r}), \tag{1}$$

where $\boldsymbol{r} = (x,y)$ are the unstrained coordinates of the carbon atoms. Notice that a critical step is to find the specific form of external forces to produce such a strain pattern. Usually, this is found by inverting the elasticity Lamé equations [26]. In graphene, this inversion to find the force load pattern has been made in some cases, like in suspended graphene [27] or to produce a uniform pseudomagnetic field [28,29]. Usually, such a step is not a trivial task. An alternative is to use the finite-size method implemented in several available software tools.

We start with an armchair graphene nanoribbon, as shown in Fig. 1, with a uniaxial strain that produces an armchair strain, and

$$\boldsymbol{u}(\boldsymbol{r}) = (u_x(y),u_y(y)) \tag{2}$$

is the corresponding strain field, which here must depend only on y. Although our approach can be applied for a general strain of the form $\boldsymbol{u}(y) = (u_x(y),u_y(y))$, here, for the sake of simplicity, we will assume that $u_x(y) = 0$ in what follows.

Let us discuss briefly the possibility of building such strain experimentally, since there is a huge asymmetry in the types of strains that can be applied to graphene [30]: while the C–C bond length can be stretched by more than 20%, it is almost incompressible because it would always change bond angle instead of shrinking bond length by out-of-plane buckling. Therefore, it is extremely hard to apply compressive strain to graphene. However, there are several ways in which the proposed strain can be realized. First the proposed strain can be made without C–C compression if the lattice is already in a state of uniform expansion and then some bonds are further stretched. In that case, only the starting interatomic distances need to be changed and our results are basically renormalized. Second, even if we assume that there is buckling in the compressed C–C bond, the out-of-plane buckling can be modeled in a first approximation as a strain field [31]. Also, it has been proved that graphene grown over certain lattices has indeed uniaxial strain [22], and of course there is always

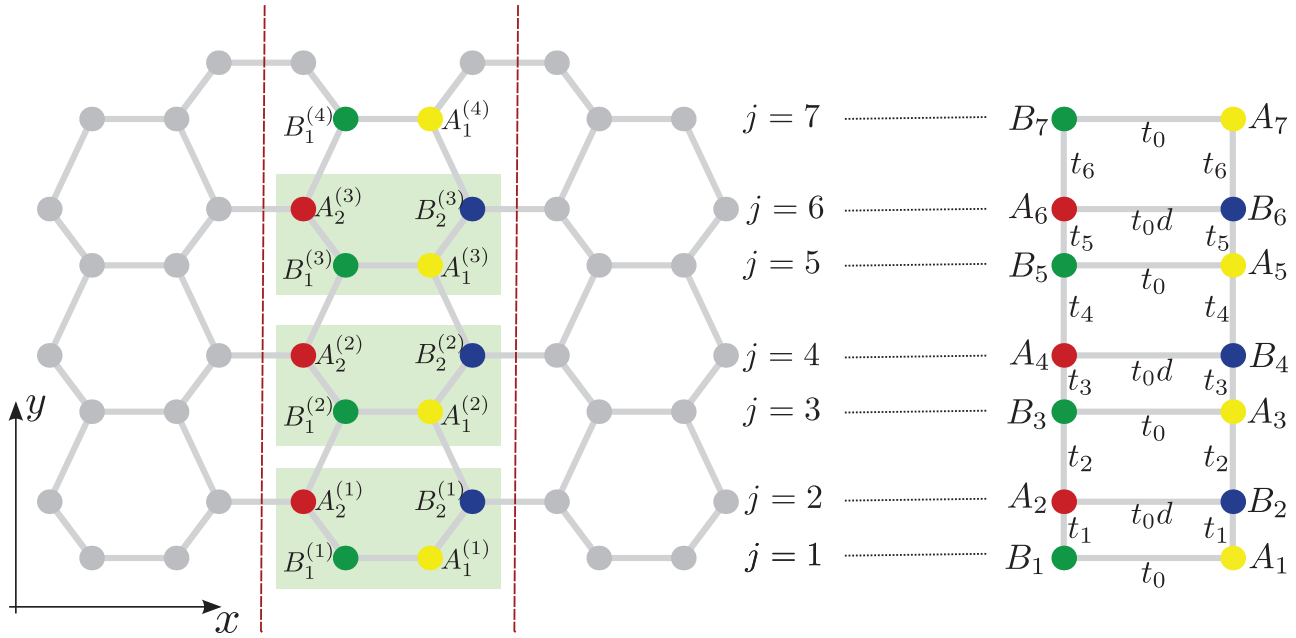

FIG. 1. (Color online) Mapping of armchair strained graphene into coupled chains. The strain in the y direction distorts the graphene hexagons, while the boundary of the unitary cell in the x direction is shown by red dotted lines. Inside of the cell, four inequivalent atoms appear (shown with different colors inside the rectangles) denoted by $A_1^{(m)}$, $A_2^{(m)}$, $B_1^{(m)}$, and $B_2^{(m)}$. The effective Hamiltonian of the armchair path in the y direction can be mapped into the coupled chains that appear to the right, where the label j corresponds to each step of the ladder along the y direction as indicated.

the possibility of building a graphene superlattice with the proposed strain.

To obtain the electronic properties, we use a one orbital next-nearest-neighbor tight-binding Hamiltonian in a honeycomb lattice, given by [32]

$$H = -\sum_{\boldsymbol{r}',n} t_{\boldsymbol{r}',\boldsymbol{r}'+\boldsymbol{\delta}'_n} c^{\dagger}_{\boldsymbol{r}'} c_{\boldsymbol{r}'+\boldsymbol{\delta}'_n} + \text{H.c.}, \tag{3}$$

where the sum over $\boldsymbol{r}'$ is taken for all sites of the deformed lattice. The vectors δ'_n point to the three next-nearest neighbors of $\boldsymbol{r}'$. For unstrained graphene $\boldsymbol{\delta}'_n = \boldsymbol{\delta}_n$, where

$$\boldsymbol{\delta}_1 = \frac{a}{2}(1,-\sqrt{3}), \quad \boldsymbol{\delta}_2 = \frac{a}{2}(1,\sqrt{3}), \quad \boldsymbol{\delta}_3 = a(-1,0), \tag{4}$$

and $c_{\boldsymbol{r}'}$ and $c^{\dagger}_{\boldsymbol{r}'}$ are the annihilation and creation operators of an electron at the lattice position $\boldsymbol{r}'$.

In such a model, the hopping integral $t_{\boldsymbol{r}',\boldsymbol{r}'+\boldsymbol{\delta}'_n}$ depends upon the strain, since the overlap between graphene orbitals is modified as the interatomic distances change. This effect can be described by [28,31]

$$t_{\boldsymbol{r}',\boldsymbol{r}'+\boldsymbol{\delta}'_n} = t_0 \exp\left[-\beta(l_{\boldsymbol{r}',\boldsymbol{r}'+\boldsymbol{\delta}'_n}/a - 1)\right], \tag{5}$$

where $l_{\boldsymbol{r}',\boldsymbol{r}'+\boldsymbol{\delta}'_n}$ is the distance between two neighbors after strain is applied. Here $\beta \approx 3$, and $t_0 \approx 2.7$ eV corresponds to graphene without strain. The unstrained bond length is denoted by a, which will be taken as $a = 1$ in what follows.

For any uniaxial armchair strain, we will prove that the Hamiltonian given by Eq. (3) can be mapped into an effective Hamiltonian made from two coupled chains, as indicated in Fig. 1. Let us show such a construction.

In nonstrained armchair nanoribbons, the lattice can be thought of as made from a periodic cell stacking [33]. Each cell has four nonequivalent atoms, as seen in Fig. 1. When uniaxial strain is applied, each cell has different strain. Thus, we introduce an index m to label cells in the y direction. The nanoribbon is now made from cells of four nonequivalent atoms with coordinates $\boldsymbol{r}'_i = (x_i^{(m)}, y_i'^{(m)})$ where $m = 1,2,3,\ldots, i = A_1, B_1, A_2, B_2$. Here, A corresponds to the sublattice A (B corresponds to sublattice B), as sketched in Fig. 1. For graphene without strain,

$$y_{A_1}^{(m)} = y_{B_1}^{(m)} = \sqrt{3}(m-1) \tag{6}$$

and

$$y_{A_2}^{(m)} = y_{B_2}^{(m)} = \sqrt{3}(m-1/2). \tag{7}$$

On each of these sites, a strain field $u_y(y)$ is applied, resulting in new positions:

$$y_i'^{(m)} = y_i^{(m)} + u_i^{(m)}, \tag{8}$$

where $u_i^{(m)}$ is a shorthand notation for $u_y(y_i^{(m)})$.

Within each chain, the nearest-neighbor orbitals are coupled by the hopping parameter $t_{AB}^{(m)}$ and have vanishing onsite energies.

For uniaxial strain, the symmetry along the x direction is not broken. Thus, the solution of the Schrödinger equation $H\boldsymbol{\Psi}(\boldsymbol{r}') = E\boldsymbol{\Psi}(\boldsymbol{r}')$ for the energy E has the form $\boldsymbol{\Psi}(\boldsymbol{r}') = \exp(ik_x x)\psi_i(m)$, where k_x is the wave vector in the x direction such that $k_x = 0,\ldots,2\pi$, $\psi_i(m)$ is the only function of $y_i^{(m)}$, where i and m label the atoms along the armchair direction, as indicated in Fig. 1. If we order the basis as $A_1^{(1)}, B_2^{(1)}, \ldots, A_1^{(N)}, B_2^{(N)}$ and $B_1^{(1)}, A_2^{(1)}, \ldots, B_1^{(N)}, A_2^{(N)}$, we obtain the following Schrödinger equation:

$$\begin{aligned}
E\psi_{A_1}(m) =& t_0\psi_{B_1}(m) + t_{A_1^{(m)}B_2^{(m)}}\psi_{B_2}(m) \\
&+ t_{A_1^{(m)}B_2^{(m-1)}}\psi_{B_2}(m-1), \\
E\psi_{B_2}(m) =& d(k_x)t_0\psi_{A_2}(m) + t_{B_2^{(m)}A_1^{(m)}}\psi_{A_1}(m) \\
&+ t_{A_1^{(m+1)}B_2^{(m)}}\psi_{A_1}(m+1), \\
E\psi_{A_2}(m) =& d^*(k_x)t_0\psi_{B_2}(m) \\
&+ t_{B_2^{(m+1)}A_2^{(m)}}\psi_{B_1}(m+1) + t_{A_2^{(m)}B_1^{(m)}}\psi_{B_1}(m), \\
E\psi_{B_1}(m) =& t_0\psi_{A_1}(m) \\
&+ t_{B_1^{(m)}A_2^{(m)}}\psi_{A_2}(m) + t_{B_1^{(m)}A_2^{(m-1)}}\psi_{A_2}(m-1),
\end{aligned} \tag{9}$$

where $d(k_x) = \exp(ik_x a)$.

Now we label the atoms as in Fig. 1, i.e., $A_1, A_2, \ldots, A_{2N}$ and $B_1, B_2, \ldots, B_{2N}$. The sequences $y_A^{(m)}$ and $y_B^{(m)}$ can be written as $y_A(j) = y_B(j) = y(j) = \sqrt{3}a(j-1)/2$ where $j = 1,2,3,\ldots,n$ labels the site number along the armchair path in the y axis. Also, we observe that, due to the uniaxial nature of the strain, several symmetries are found in the bonds, $t_{A_1^{(m)}B_2^{(m)}} = t_{B_1^{(m)}A_2^{(m)}}$ as well as $t_{A_2^{(m)}B_1^{(m+1)}} = t_{B_2^{(m)}A_1^{(m+1)}}$, which allows us to reduce the resulting Schrödinger equation.

Finally, the Hamiltonian is mapped into a new one, $H(k_x)$, without any reference to cells of four sites:

$$\begin{aligned}
H(k_x) =& \sum_j t_0[d(k_x)a_{2j}^{\dagger}b_{2j} + a_{2j+1}^{\dagger}b_{2j+1}] \\
&+ \sum_j t_j a_j^{\dagger} b_{j+1} + \text{H.c.},
\end{aligned} \tag{10}$$

where a_j, $a_j^{\dagger}$, and a_j, $b_j^{\dagger}$ are the annihilation and creation operators in the lattices A and B, respectively. This effective Hamiltonian describes two modulated chains coupled by bonds of strength t_0 and $t_0 d(k_x)$, as sketched out in Fig. 1, where t_j are the values of the transfer integrals along the chains in the y direction. They are obtained as follows.

First, we calculate the length between atoms after strain is applied:

$$l_{\boldsymbol{r}',\boldsymbol{r}'+\boldsymbol{\delta}'_n} = ||\boldsymbol{\delta}_n + \boldsymbol{u}(\boldsymbol{r}+\boldsymbol{\delta}_n) - \boldsymbol{u}(\boldsymbol{r})||. \tag{11}$$

In the present case, two different kinds of bond lengths are obtained:

$$\begin{aligned}
&l_{A_1^{(m)},B_2^{(m+s)}} \\
&= \sqrt{\left(\delta_{s+2}^x\right)^2 + \left[\delta_{s+2}^y + u_y\left(y_{B_2^{(m+s)}}\right) - u_y\left(y_{A_1^{(m)}}\right)\right]^2},
\end{aligned} \tag{12}$$

where $s = 0,-1$. δ_{s+2}^x and δ_{s+2}^y denote the x and y components of each of the vectors $\boldsymbol{\delta}_1$ and $\boldsymbol{\delta}_2$.

Thus, for *odd* values of j,

$$t_j = t_0 \exp\left[-\beta\left(l_{A_1^{(j+1)/2},B_2^{(j+1)/2}} - 1\right)\right], \tag{13}$$

while, for *even* values of j,

$$t_j = t_0 \exp\left[-\beta\left(l_{A_1^{(j/2)},B_2^{(j/2+1)}} - 1\right)\right]. \tag{14}$$

In order to compare with other works, the case of small strain is interesting. Under such approximation, the hopping parameter between nearest neighbors along the chain is simplified a lot:

$$t_j \approx t_0 \exp\left[-\sqrt{3}\beta(u_{j+1} - u_j)/2\right], \tag{15}$$

where it is understood that u_j is the displacement of the jth atom along the vertical armchair path, i.e., $u_j = u_i^{(m)}$. However, in the literature the most common approach is to use a linear approximation for the hopping parameter, given by

$$t_j \approx t_0 \left[1 - \frac{\sqrt{3}\beta}{2}(u_{j+1} - u_j)\right]. \tag{16}$$

Summarizing, Eq. (10) is an effective one-dimensional Hamiltonian with effective hopping parameters given by Eqs. (13) and (14). For small strain amplitude, Eqs. (13) and (14) are replaced by their linearized version, Eq. (16). Such a set of equations maps any uniaxial armchair strain into a pair of coupled chains.

III. PERIODIC ARMCHAIR STRAIN

To understand the rich physics involved in strain, let us now concentrate on the case of periodic strain, which arises when graphene is grown on top of a substrate with a different lattice parameter [14]. The simplest choice is to consider a sinusoidal kind of strain, similar to the observed pattern in graphene grown over iron [14]. This imposed oscillation contains three parameters: wavelength (controlled by the parameter σ), amplitude (controlled by λ), and phase (controlled by ϕ). In order to simplify the resulting equations, we prefer to write the oscillating strain as

$$u_y(y) = \frac{\lambda}{\sqrt{3}\beta} \cos\left[\frac{4\pi\sigma}{\sqrt{3}}(y - \sqrt{3}/4) + \phi\right]. \tag{17}$$

Figure 2 shows the complex spectrum of H as a function of σ, obtained using fixed boundary conditions and by diagonalizing the resulting matrix for each value of k_x. The calculation presented here was made for a width of 160 atoms, and in Fig. 3 we present the resulting spectra for smaller sizes.

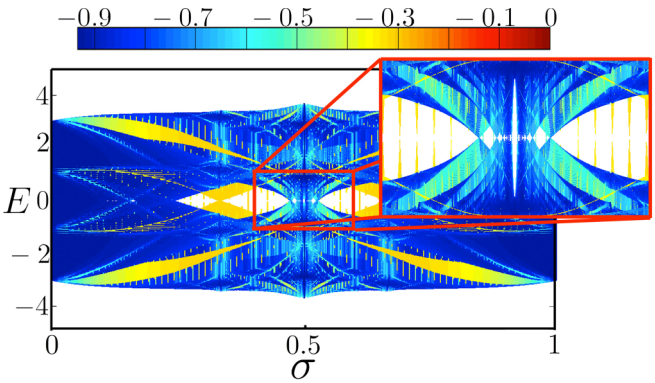

FIG. 2. (Color online) Spectrum as a function of σ for $\lambda = 1$ and $\phi = \pi\sigma$ obtained by solving the Schrödinger equation for a system of 160 atoms, using 250 grid points for sampling k_x and with fixed boundary conditions. The different colors represent the normalized localization participation ratio $\alpha(E)$. Inset: $\sigma = 1/2$ near $E = 0$.

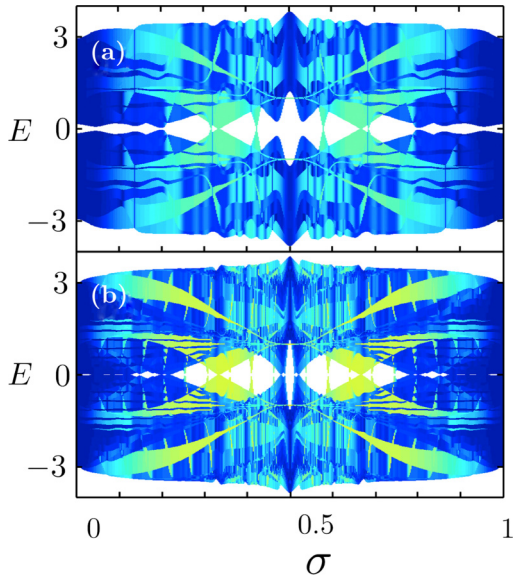

FIG. 3. (Color online) Spectrum as a function of σ for $\lambda = 1$ and $\phi = \pi\sigma$ obtained by solving the Schrödinger equation for a system of (a) 20 atoms and (b) 40 atoms, using 250 grid points for sampling k_x and with fixed boundary conditions. The different colors represent the normalized localization participation ratio $\alpha(E)$.

As expected, the gaps are amplified for smaller sizes due to quantum confinement effects [33,34], although there are fluctuations associated with the width, as happens with pure graphene nanoribbons [33]. Also, within our method it is possible to get bulk graphene by imposing periodic boundary conditions in the y direction, as will be done for the case $\sigma = 1/2$.

The most important feature of the resulting spectrum is its fractal nature, which is akin to the Hofstadter butterfly [18] which arises in the case of a lattice under a uniform magnetic field [17]. To illustrate this, we included color in Fig. 2 to code the localization properties of the wave functions. They are studied by calculating the normalized participation ratio, defined as

$$\alpha(E) = \frac{\ln \sum_{j=1}^{N} |\psi(j)|^4}{\ln N}. \tag{18}$$

The quantity $\alpha(E)$ estimates the occupied area by an electronic state [35]. For extended states, $\alpha(E) \to -1$ (blue color in the figure), while it tends to be bigger when localization is presented (red color in the figure). In the spectrum, it is clearly seen how different localizations coexist, making a very complex system in this respect.

To have a better understanding of the spectrum and its relationship with the Hofstadter buttery, it is useful to consider the small strain case. Using Eq. (16), the hopping integrals along the chains are given by

$$t_j = t_0 \left[1 + \lambda \sin(\pi\sigma) \sin(2\pi\sigma j + \phi)\right]. \tag{19}$$

We recognize that Eq. (19) corresponds to the transfer integrals of the off-diagonal Harper model [17], that produces a Hofstadter butterfly [18]. The main difference here is that we have an off-diagonal Harper ladder.

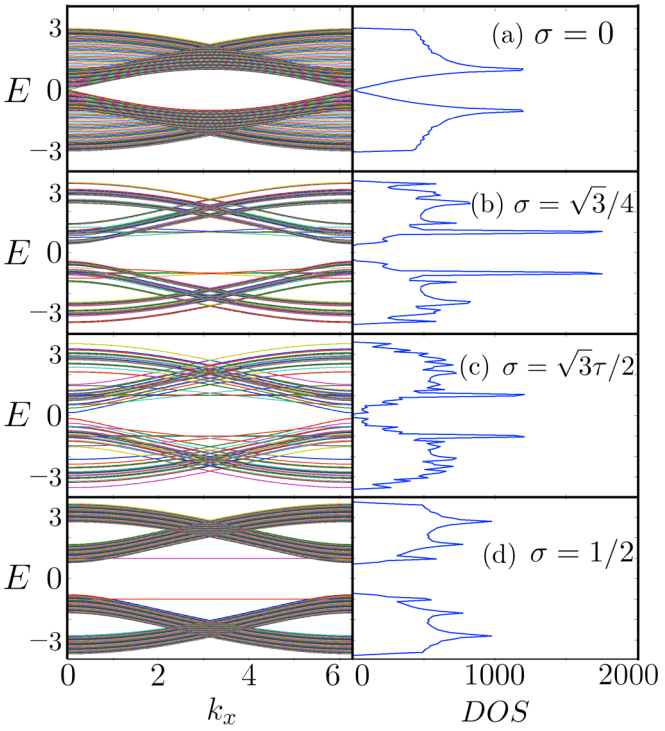

FIG. 4. (Color online) Band structure (left column) and density of states (right column) using $\phi = \pi\sigma$ and $\lambda = 1$ for (a) an unstrained graphene lattice, (b) strained graphene with $\sigma = \sqrt{3}/4$, (c) strained graphene with $\sigma = \sqrt{3}\tau/2$, and (d) strained graphene with $\sigma = 1/2$. Fixed boundary conditions were used in this plot.

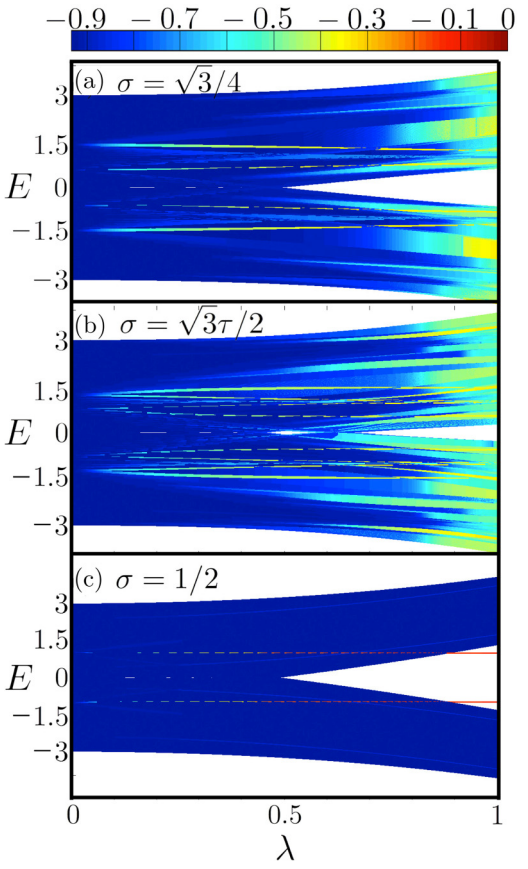

FIG. 5. (Color online) Energy spectrum of graphene as a function of λ for (a) $\sigma = \sqrt{3}/4$, (b) $\sigma = \sqrt{3}\tau/2$, and (c) $\sigma = 1/2$. For $\lambda > 1/2$ a gap at the Fermi level is opened. Fixed boundary conditions were used in this plot.

As in the Harper model, the fractal nature of the spectrum is given by the number theory properties of σ. When σ is a rational number, say $\sigma = P/Q$, the effective one-dimensional potential has a superperiod Q. Thus states have a Bloch nature. For irrational σ, the potential is *quasiperiodic*. Although the Bloch theorem is still valid, it does not provide any reduction of the problem since an infinite number of reciprocal space components are needed to generate the wave function [18]. This can generate a cascade of gaps or critical eigenstates [36]. Interestingly, in the Harper model, the gaps have a topological nature [36–40]. Moreover, since the problem of finding the solutions to a quasiperiodic potential is akin to the small divisor problem in dynamical systems [41], perturbation theory has a very limited value. A sequence of rational approximates or renormalization techniques are much better strategies to follow [41–44].

It is also interesting to discuss the resulting bands as a function of k_x, using different values of σ at a fixed lambda. In Fig. 4 we present the bands with the corresponding density of states (DOS) to the right. For $\sigma = 0$ we recover the graphene case, where the Dirac cones projections are seen at $E = 0$, resulting in a linear DOS at the Fermi level. However, for the three selected cases, $\sigma = \sqrt{3}/4$, $\sigma = \sqrt{3}\tau/2$, and $\sigma = 1/2$, the Dirac cones are completely destroyed. The DOS for the case $\sigma = 1/2$ suggests that the problem is akin to two uncoupled linear chains. As we will see, these two chains are not the ones that are observed to the right in Fig. 1, since t_0 and $t_0 d$ are never zero. These effective chains are in fact running in the x direction, due to the fact that for some $j > 0$ we can have $t_j \approx 0$ or even $t_j = 0$. Also, two edge states are observed at $E = \pm 1$. These states are the remaining of the original Van Hove singularities that appear at the same energy for unstrained graphene. The other cases for irrational σ are spiky, as was also observed and explained in our work of zig-zag strain [16]. This is due to the quasiperiodic behavior of the resulting potential for irrational σ, which results in many nearly uncoupled linear chains of different widths [16]. Thus, the DOSs are strikingly similar to those observed in narrow nanoribbons [45].

Consider now how the spectrum changes with λ for a given σ. Figure 5 presents such evolution for fixed boundary conditions. The main result here is the big gap opening at the Fermi level for the different σ as λ grows. When compared with the zig-zag case [16], is clear that armchair strain is much more efficient to produce gaps, especially at the Fermi level. Also, the case $\sigma = 1/2$ shows two edge states at $E = \pm 1$ which have a topological nature, as will be discussed in a special section.

IV. HALF-FILLING CASE $\sigma = 1/2$: MIXING DIRAC AND SCHRÖDINGER FERMIONS

Of particular interest is the case $\sigma = 1/2$, which for topological insulators is associated with half filling of the bands. For this case, the main interest is to know if a gap

is open or not. We start by noting that the hopping parameter can be written, using Eq. (19), as

$$t_j = 1 + (-1)^j \lambda. \tag{20}$$

This results in a staggered ladder in which the unitary cell contains only four nonequivalent atoms. As a result, the effective Hamiltonian can be further reduced using the symmetry in the y axis. For that end, the wave function can be written as

$$\Psi(\boldsymbol{r}') = \exp(ik_x x)\exp(ik_y y)\psi_i(j), \tag{21}$$

where now $j = 1,2$. The corresponding spectrum is found by looking at the eigenvalues of the 4×4 effective matrix Hamiltonian, whose solutions, in terms of the parameters λ, k_x, and k_y, are given by

$$E_{\pm,\pm} = \pm\sqrt{\mp 2\sqrt{-(1+\cos k_x)g(\lambda,k_y)} \mp [-1 - 2g(\lambda,k_y)]}, \tag{22}$$

where

$$g(\lambda,k_y) = -1 - \lambda^2 + (\lambda^2 - 1)\cos\left(\frac{\sqrt{3}k_y}{2}\right). \tag{23}$$

The gap size Δ can be found by minimizing the square of the energy in Eq. (22), since the bands are symmetric around $E = 0$. The momentums that produce a minimum are $k_x = 2n\pi$ and $k_y = 2\pi(2n+1)/\sqrt{3}$, where $n = 0,1,2,\ldots,n$. The resulting gap is given by

$$\Delta = 4\left(\lambda - \tfrac{1}{2}\right) \tag{24}$$

and grows linearly with λ. This gap opening can be confirmed in Fig. 5. Notice, however, that the linear behavior is seen only near $\lambda = 1/2$, mainly because Fig. 5 was made for the nonlinearized model.

Furthermore, at the critical point $\lambda = \lambda_c = 1/2$ in which the spectrum changes from nongapped to gapped, we obtained a very interesting behavior. In Fig. 6, we plot the dispersion relationship $E_{\pm,\pm}$ as a function of k_x and k_y. As one can see, at the Fermi level there is a kind of Dirac point at $\boldsymbol{K} = (0, 2\pi(2n+1)/\sqrt{3})$. However, it is not a cone. Instead, in the k_x direction the behavior is linear, i.e., of the Dirac type, while in the k_y direction it behaves in a parabolic fashion; i.e., the fermions follow the usual Schrödinger behavior. For $\lambda = \lambda_c$, and near the Dirac point, one can confirm such behavior by expanding Eq. (22) in series. In the k_x direction [$k_y = 2\pi(2n+1)/\sqrt{3}$] we find the Dirac behavior,

$$E_{\pm,\pm} = \pm\frac{k_x}{2}, \tag{25}$$

while in the k_y direction ($k_x = 0$) we find a Schrödinger behavior:

$$E_{\pm,\pm} = \pm\frac{9}{32}\left[k_y - \frac{2\pi}{\sqrt{3}}(2n+1)\right]^2. \tag{26}$$

Thus, this highlights the paramount importance of the particular half-filling and half-amplitude $\sigma = \lambda = 1/2$ critical point, in which the electron has a mixed Dirac and Schrödinger fermion dynamics, as seen in Fig. 6. The reason for this transition can be understood by looking at the limiting cases. For $\lambda = 0$, the system is unstrained graphene in which

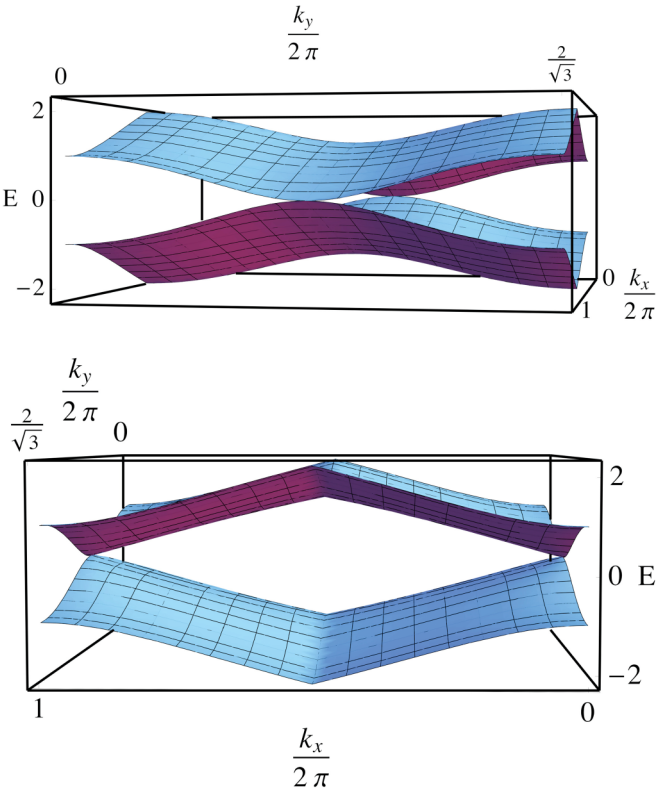

FIG. 6. (Color online) Different perspectives of the energy surface as a function of k_x and k_y for $\lambda = 1/2$ and $\sigma = 1/2$, using a linearized version of t_j. Notice how the electron has a mixed Schrödinger parabolic behavior with a Dirac linear fermion behavior at the Fermi level corresponding to $E = 0$.

electrons behave as Dirac fermions. At $\lambda = 1$, $t_j = 0$ for j odd, resulting in a decoupled system in the y direction. The system is thus made of two-atom-width nanoribbons spanning the x direction. In this case, the particles follow a chainlike behavior, i.e., of the Schrödinger type. As λ decreases, the parallel chains have a small interaction, as is suggested by the DOSs that appear in Fig. 4(d), which corresponds to two linear chains. Thus, the critical point separates two regions of different effective dimensionality. One is mainly two dimensional while in the other the propagation is nearly unidimensional. From a different point of view, this transition is due to the merging of Dirac cones, as was suggested in previous works by tuning *ad hoc* the transfer integrals [20,21]. In Fig. 7, we present three stages of the dispersion relationship evolution near the critical point. Below λ_c, two Dirac cones are seen, which are merged at $\lambda = \lambda_c$. Then a gap is open for $\lambda > \lambda_c$. Notice that the mixing of Dirac-Schrödinger dynamics is not observable using the zig-zag case, since the effective chain never has only two kinds of bonds [16].

V. TOPOLOGICAL STATES

As was discussed previously, in Figs. 4(d) and 5(c), two flat bands are seen at $E = \pm 1$ when $\sigma = 1/2$. These two bands only appear when fixed boundary conditions are considered, since the energy dispersion for the bulk given by Eq. (22)

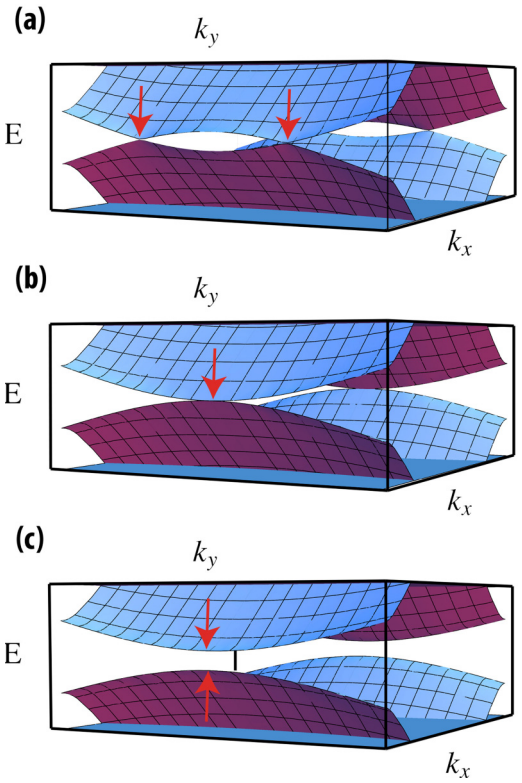

FIG. 7. (Color online) Evolution of the energy surface as a function of k_x and k_y for $\sigma = 1/2$ near the critical point. (a) $\lambda = 0.9\lambda_c$. (b) $\lambda = \lambda_c$. (c) $\lambda = 1.1\lambda_c$. In case (a), two Dirac cones are seen, which are merged in (b), and in (c) the cones disappear. The arrows indicate the position of the Fermi level.

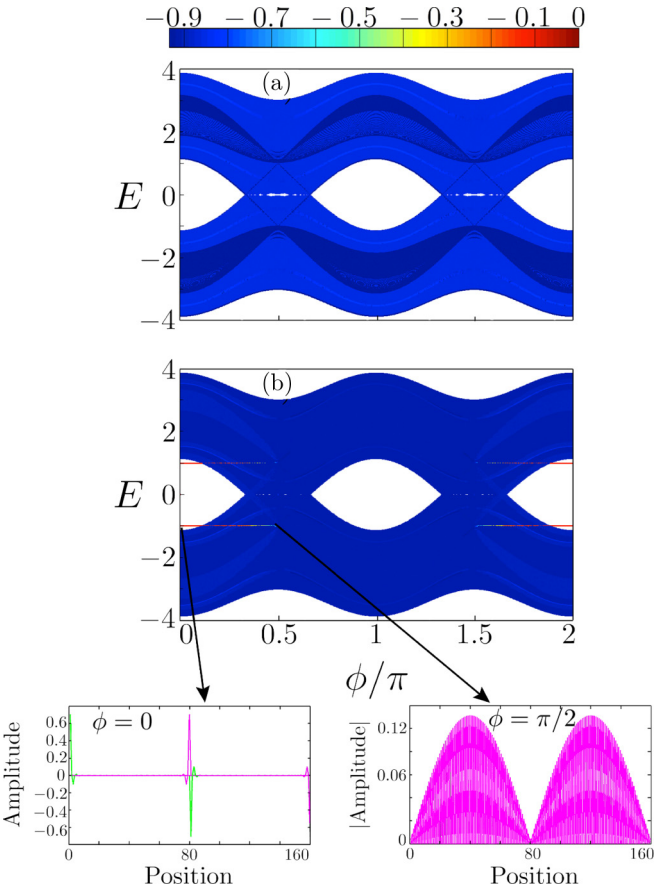

FIG. 8. (Color online) Upper panels show the energy spectrum with 160 sites with $\lambda = \lambda_C$ and $\sigma = 1/2$. (a) Energy spectrum using cyclic boundary conditions. (b) Energy spectrum using fixed boundary conditions. The colors represent the normalized localization participation ratio $\alpha(E)$. Two $E = \pm 1$ energy modes are localized on either one of the edges and on the middle of the chain in $0 \leqslant \phi < \pi/2$. For $\phi = \pi/2$ the localized energy modes become extended. The lower panel displays the eigenstates for $E = -1$ energy modes using $\phi = 0$ and $\pi/2$. Notice how the wave function is modulated with an envelope of bigger wavelength, a phenomena called Chern beating [19].

does not present such states as seen in Fig. 8. Thus, these are edge states. It is well known that systems with band gaps and edge states can present nontrivial topological properties [46]. Here we decided to look at the behavior of the spectrum as a function of the phase in the potential, given by ϕ in Eq. (17).

In Fig. 8 we present the spectrum for the bulk and when fixed boundary conditions are included, as a function of the phase ϕ for $\sigma = 1/2$ and $\lambda = \lambda_c$. As we can see, the edge states present a nontrivial topological behavior, since they are absent in one of the gaps. We can track the behavior of the related states as seen in Fig. 8. For ϕ close to zero, the states are localized at the edges as expected, but surprisingly they also have amplitude near the center. However, this can be explained by observing that in this limit we almost have chain decoupling. Thus, these states are edge states of the effective one-dimensional system, which seems to be a very interesting phenomenon. Furthermore, observe how the amplitudes are interlaced at the center, due to the symmetry of the problem. As the phase moves, these states eventually merge with the band edges, near $\phi = \pi/2$, and present a nonlocalized nature. As shown in the figure, the wavefunction spatial pattern seems to be sinusoidal with a long-wave modulation, which suggests that the Chern beating effect, originally observed and explained in quasiperiodic systems [19], is also present here.

VI. CONCLUSIONS

In conclusion, we provided a general way to map any uniaxial armchair strain into an effective one-dimensional system. For the particular case of periodic strain, we obtained a spectrum akin to the Hofstadter butterfly. The armchair strain produces bigger gaps than the zigzag case. An analysis of the half -filling case for the periodic strain reveals a critical point for the opening of the gap. At this critical point, the fermions have a mixed behavior. In one direction they behave with a Dirac dynamics, while in the perpendicular one they follow a Schrödinger one. Such behavior arises as a consequence of a change in the effective dimensionality of the system. Also, we have observed some topological states due to strain. Interestingly, strain allows us to have some amplitude of the topological modes inside the bulk through a decoupling of the system. These states also present the phenomenon of Chern beating observed in other quasiperiodic systems [19]. This opens the avenue for a whole set of new phenomena that seems to be realizable from an experimental point of view.

ACKNOWLEDGMENTS

We thank Indu Satija and Maurice Oliva-Leyva for enlightening discussions and a critical reading of the manuscript. This work was supported by the Dirección General de Asuntos del Personal Académico-Programa de Apoyo a Proyectos de Investigación e Innovación Tecnológica (DGAPA-PAPIIT) IN-102513 project, and by the Dirección General de Cómputo y de Tecnologías de Información y Comunicación (DGTIC)-NES center. P.R.-T. acknowledges support from Consejo Nacional de Ciencia y Tecnología (CONACYT) (Mexico).

[1] K. S. Novoselov, A. K. Geim, S. V. Morozov, D. Jiang, Y. Zhang, S. V. Dubonos, I. V. Grigorieva, and A. A. Firsov, Science **306**, 666 (2004).
[2] C. Lee, X. Wei, J. W. Kysar, and J. Hone, Science **321**, 385 (2008).
[3] V. M. Pereira, A. H. Castro Neto, and N. M. R. Peres, Phys. Rev. B **80**, 045401 (2009).
[4] V. M. Pereira and A. H. Castro Neto, Phys. Rev. Lett. **103**, 046801 (2009).
[5] F. Guinea, Solid State Commun. **152**, 1437 (2012).
[6] D. Zhan, J. Yan, L. Lai, Z. Ni, L. Liu, and Z. Shen, Advanced Materials **24**, 4055 (2012).
[7] C. Si, Z. Liu, W. Duan, and F. Liu, Phys. Rev. Lett. **111**, 196802 (2013).
[8] H. Suzuura and T. Ando, Phys. Rev. B **65**, 235412 (2002).
[9] A. A. Pacheco Sanjuan, Z. Wang, H. Pour Imani, M. Vanević, and S. Barraza-Lopez, Phys. Rev. B **89**, 121403(R) (2014).
[10] J. L. Mañes, Phys. Rev. B **76**, 045430 (2007).
[11] A. F. Morpurgo and F. Guinea, Phys. Rev. Lett. **97**, 196804 (2006).
[12] M. Vozmediano, M. Katsnelson, and F. Guinea, Physics Reports **496**, 109 (2010).
[13] M. Oliva-Leyva and G. G. Naumis, Phys. Rev. B **88**, 085430 (2013).
[14] N. A. Vinogradov, A. A. Zakharov, V. Kocevski, J. Rusz, K. A. Simonov, O. Eriksson, A. Mikkelsen, E. Lundgren, A. S. Vinogradov, N. Mårtensson, and A. B. Preobrajenski, Phys. Rev. Lett. **109**, 026101 (2012).
[15] C. R. Woods, L. Britnell, A. Eckmann, R. S. Ma, J. C. Lu, H. M. Guo, X. Lin, G. L. Yu, Y. Cao, R. V. Gorbachev, A. V. Kretinin, J. Park, L. A. Ponomarenko, M. I. Katsnelson, Y. Gornostyrev, K. Watanabe, T. Taniguchi, C. Casiraghi, H. J. Gao, A. K. Geim, and K. S. Novoselov, Nat. Phys. **10**, 451 (2014).
[16] G. G. Naumis and P. Roman-Taboada, Phys. Rev. B **89**, 241404 (2014).
[17] P. G. Harper, Proc. Phys. Soc. London, Sect. A **68**, 874 (1955).
[18] D. R. Hofstadter, Phys. Rev. B **14**, 2239 (1976).
[19] I. I. Satija and G. G. Naumis, Phys. Rev. B **88**, 054204 (2013).
[20] L.-K. Lim, J.-N. Fuchs, and G. Montambaux, Phys. Rev. Lett. **108**, 175303 (2012).
[21] G. Montambaux, F. Piéchon, J.-N. Fuchs, and M. O. Goerbig, Phys. Rev. B **80**, 153412 (2009).
[22] G.-X. Ni, H.-Z. Yang, W. Ji, S.-J. Baeck, C.-T. Toh, J.-H. Ahn, V. M. Pereira, and B. Zyilmaz, Advanced Materials **26**, 1081 (2014).
[23] T. Uehlinger, G. Jotzu, M. Messer, D. Greif, W. Hofstetter, U. Bissbort, and T. Esslinger, Phys. Rev. Lett. **111**, 185307 (2013).
[24] U. Kuhl, S. Barkhofen, T. Tudorovskiy, H.-J. Stöckmann, T. Hossain, L. de Forges de Parny, and F. Mortessagne, Phys. Rev. B **82**, 094308 (2010).
[25] O. Peleg, G. Bartal, B. Freedman, O. Manela, M. Segev, and D. N. Christodoulides, Phys. Rev. Lett. **98**, 103901 (2007).
[26] A. Sommerfeld, *Mechanics of Deformable Bodies: Lectures on Theoretical Physics*, Lectures on Theoretical Physics (Academic, New York, 1950).
[27] J. C. Meyer, A. K. Geim, M. I. Katsnelson, K. S. Novoselov, T. J. Booth, and S. Roth, Nature (London) **446**, 60 (2007).
[28] F. Guinea, M. I. Katsnelson, and A. K. Geim, Nat. Phys. **6**, 30 (2010).
[29] T. Low and F. Guinea, Nano Lett. **10**, 3551 (2010).
[30] Y. Zhang and F. Liu, Appl. Phys. Lett. **99**, 241908 (2011).
[31] R. M. Ribeiro, V. M. Pereira, N. M. R. Peres, P. R. Briddon, and A. H. C. Neto, New Journal of Physics **11**, 115002 (2009).
[32] W. Lu, P. Soukiassian, and J. Boeckl, MRS Bulletin **37**, 1119 (2012).
[33] A. Cresti, N. Nemec, B. Biel, G. Niebler, F. Triozon, G. Cuniberti, and S. Roche, Nano Research **1**, 361 (2008).
[34] G. G. Naumis, M. Terrones, H. Terrones, and L. M. Gaggero-Sager, Appl. Phys. Lett. **95**, 182104 (2009).
[35] G. G. Naumis, Phys. Rev. B **76**, 153403 (2007).
[36] G. G. Naumis and F. Lpez-Rodrguez, Physica B: Condensed Matter **403**, 1755 (2008).
[37] S. Ganeshan, K. Sun, and S. Das Sarma, Phys. Rev. Lett. **110**, 180403 (2013).
[38] M. Verbin, O. Zilberberg, Y. E. Kraus, Y. Lahini, and Y. Silberberg, Phys. Rev. Lett. **110**, 076403 (2013).
[39] Y. E. Kraus and O. Zilberberg, Phys. Rev. Lett. **109**, 116404 (2012).
[40] L.-J. Lang, X. Cai, and S. Chen, Phys. Rev. Lett. **108**, 220401 (2012).
[41] D. DiVincenzo and P. Steinhardt, *Quasicrystals: The State of the Art, Series on Directions in Condensed Matter Physics* (World Scientific, Singapore, 1999).
[42] G. G. Naumis and J. L. Aragón, Phys. Rev. B **54**, 15079 (1996).
[43] G. G. Naumis, Phys. Rev. B **59**, 11315 (1999).
[44] R. Nava, J. Tagea-Martnez, J. A. del Ro, and G. G. Naumis, Journal of Physics: Condensed Matter **21**, 155901 (2009).
[45] K. Nakada, M. Fujita, G. Dresselhaus, and M. S. Dresselhaus, Phys. Rev. B **54**, 17954 (1996).
[46] X.-L. Qi and S.-C. Zhang, Rev. Mod. Phys. **83**, 1057 (2011).